



## Reverse-absorbance-modulation-optical lithography for optical nanopatterning at low light levels

Apratim Majumder, Xiaowen Wan, Farhana Masid, Benjamin J. Pollock, Trisha L. Andrew, Olivier Soppera, and Rajesh Menon

Citation: *AIP Advances* **6**, 065312 (2016); doi: 10.1063/1.4954178

View online: <http://dx.doi.org/10.1063/1.4954178>

View Table of Contents: <http://scitation.aip.org/content/aip/journal/adva/6/6?ver=pdfcov>

Published by the *AIP Publishing*

---

### Articles you may be interested in

[A comprehensive simulation model of the performance of photochromic films in absorbance-modulation-optical-lithography](#)

*AIP Advances* **6**, 035210 (2016); 10.1063/1.4944489

[Enhancing optical power of GaN-based light-emitting diodes by nanopatterning on indium tin oxide with tunable fill factor using multiple-exposure nanosphere-lens lithography](#)

*J. Appl. Phys.* **116**, 194301 (2014); 10.1063/1.4901829

[Light modulation with nanopatterned diffractive microelectromechanical system pixels](#)

*J. Vac. Sci. Technol. B* **26**, 2139 (2008); 10.1116/1.2998725

[Spatial light modulator for maskless optical projection lithography](#)

*J. Vac. Sci. Technol. B* **24**, 2852 (2006); 10.1116/1.2387156

[Spatial light modulation by nonlinear absorbers](#)

*J. Appl. Phys.* **66**, 61 (1989); 10.1063/1.343858

---

Searching? Trust CISE.

It's peer-reviewed and appears in the IEEE Xplore and AIP library packages.

## Reverse-absorbance-modulation-optical lithography for optical nanopatterning at low light levels

Apratim Majumder,<sup>1,a,b</sup> Xiaowen Wan,<sup>1,b</sup> Farhana Masid,<sup>1</sup> Benjamin J. Pollock,<sup>2</sup> Trisha L. Andrew,<sup>2</sup> Olivier Soppera,<sup>3</sup> and Rajesh Menon<sup>1</sup>

<sup>1</sup>Department of Electrical and Computer Engineering, University of Utah, Salt Lake City, Utah 84112, USA

<sup>2</sup>Department of Chemistry, University of Wisconsin-Madison, Madison, Wisconsin 53706, USA

<sup>3</sup>Mulhouse Institute for Material Sciences, CNRS LRC 7228, BP2488, Mulhouse 68200, France

(Received 12 April 2016; accepted 5 June 2016; published online 13 June 2016)

Absorbance-Modulation-Optical Lithography (AMOL) has been previously demonstrated to be able to confine light to deep sub-wavelength dimensions and thereby, enable patterning of features beyond the diffraction limit. In AMOL, a thin photochromic layer that converts between two states via light exposure is placed on top of the photoresist layer. The long wavelength photons render the photochromic layer opaque, while the short-wavelength photons render it transparent. By simultaneously illuminating a ring-shaped spot at the long wavelength and a round spot at the short wavelength, the photochromic layer transmits only a highly confined beam at the short wavelength, which then exposes the underlying photoresist. Many photochromic molecules suffer from a giant mismatch in quantum yields for the opposing reactions such that the reaction initiated by the absorption of the short-wavelength photon is orders of magnitude more efficient than that initiated by the absorption of the long-wavelength photon. As a result, large intensities in the ring-shaped spot are required for deep sub-wavelength nanopatterning. In this article, we overcome this problem by using the long-wavelength photons to expose the photoresist, and the short-wavelength photons to confine the “exposing” beam. Thereby, we demonstrate the patterning of features as thin as  $\lambda/4.7$  (137nm for  $\lambda = 647\text{nm}$ ) using extremely low intensities (4-30 W/m<sup>2</sup>, which is 34 times lower than that required in conventional AMOL). We further apply a rigorous model to explain our experiments and discuss the scope of the reverse-AMOL process. © 2016 Author(s). All article content, except where otherwise noted, is licensed under a Creative Commons Attribution (CC BY) license (<http://creativecommons.org/licenses/by/4.0/>). [<http://dx.doi.org/10.1063/1.4954178>]

### I. INTRODUCTION

Optical lithography is arguably the key enabling technology of the semiconductor industry.<sup>1-5</sup> The diffraction limit<sup>6</sup> associated with all optical systems, has been circumvented by a number of techniques like self-aligned patterning techniques,<sup>7,8</sup> multiple exposure-and-etch mechanisms<sup>9</sup> and a number of other near-field methods<sup>10-13</sup> that have been inspired by techniques of super-resolution nanoscopy like stimulated-emission-depletion (STED).<sup>14</sup> Most of these techniques suffer from increased cost, complexity<sup>15</sup> or very high intensities.<sup>11-13</sup> Additionally, there has also been advances in pushing the resolution limit by employing plasmonics-based approaches,<sup>16-18</sup>

<sup>a</sup>E-mail: [apratim.majumder@utah.edu](mailto:apratim.majumder@utah.edu)

<sup>b</sup>These authors contributed equally to this work.



most of which require precise control of sample-mask gap since these are primarily near-field effect based techniques. Our approach to super-resolution nanopatterning, termed absorbance-modulation-optical lithography (AMOL)<sup>19–21</sup> has experimentally demonstrated patterning beyond the diffraction limit,<sup>22–24</sup> by enabling near-field lithography by means of far-field optics.

Traditionally, in AMOL, a thin layer of photochromic molecules called the absorbance modulation layer (AML), with the ability to reversibly photo-transition based on the wavelength of illumination (Fig. 1(a)), is used to achieve super-resolution nanopatterning. As illustrated in Fig. 1(b), a peak in the “exposing” beam ( $\lambda_1$ ) and a node in the “confining” beam ( $\lambda_2$ ) simultaneously illuminate the AML. The resulting photo-transitions in the AML effectively confine the “exposing” beam to a deep-subwavelength region, which exposes the underlying photoresist. In this case, the photoresist is chosen such that the “confining” beam does not affect it.

Diarylethenes such as 1,2-bis(5,5’-dimethyl-2,2’-bithiophen-4-yl) perfluorocyclopent-1-ene (otherwise referred to as BTE) are ideal molecules for the AML due to their stability. However, the quantum efficiency of the “exposing” reaction is about 3 orders of magnitude larger than that of the “confining” reaction.<sup>22–24</sup> This necessitates the intensity in the “confining” beam to be correspondingly larger for deep sub-wavelength patterning. Here, we avoid this problem by switching the wavelengths used for the “exposing” and “confining” beams, a technique we refer to as reverse-AMOL. The technique is illustrated on the right in Fig. 1(b). In this case, we need to utilize a photoresist that is sensitive to the longer wavelength,  $\lambda_2$ , while not being affected by the shorter wavelength,  $\lambda_1$ . The details of the experimental process are described later.

We first begin by using a previously developed rigorous model<sup>21</sup> to simulate the performance of reverse-AMOL. The model utilizes finite-element-method (FEM) (COMSOL interfaced with MATLAB) to model the photochemical reactions and light propagation that occur inside the AML.

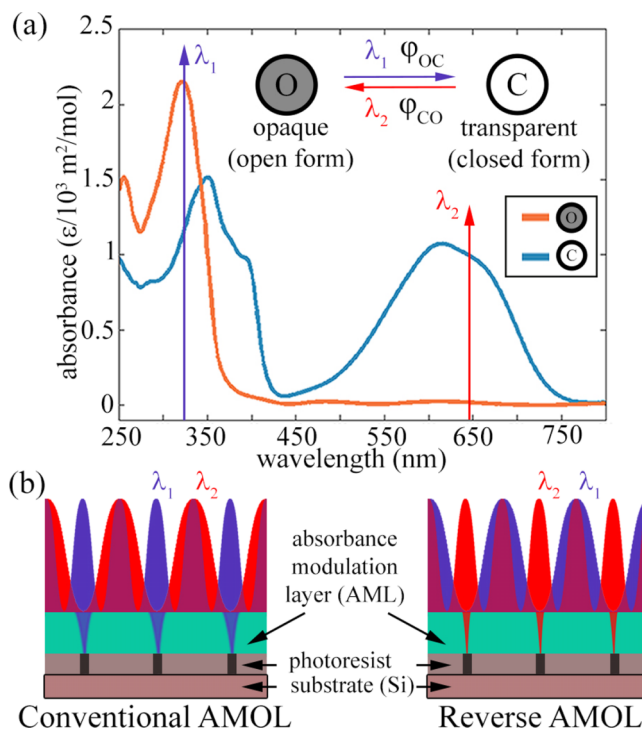


FIG. 1. (a) UV-Vis absorbance spectra of the diarylethene molecule, BTE showing the confining ( $\lambda_2 = 647$  nm) and exposing beam ( $\lambda_1 = 325$  nm) wavelengths. Reprinted with permission from AIP Advances 6, 035210 (2016). Copyright 2016 Author(s), licensed under a Creative Commons Attribution 4.0 License. (Inset) Scheme of the photoreaction. (b) Schematic of conventional AMOL showing simultaneous illumination of the AML by standing waves of  $\lambda_2$  and  $\lambda_1$ . Reprinted with permission from AIP Advances 6, 035210 (2016). Copyright 2016 Author(s), licensed under a Creative Commons Attribution 4.0 License. Reverse-AMOL where the illumination scheme is reversed and  $\lambda_2$  acts as the exposing beam and  $\lambda_1$  acts as the confining beam.

Such a model has been previously used<sup>21,25,26</sup> to elucidate the effect of the material properties, light polarization, etc. in AMOL and demonstrated to be highly successful in handling dispersive and inhomogeneous media such as the AML and solving Maxwell's equations based on user defined material properties. Details of the model specific to reverse-AMOL and relevant mathematical derivations are described in the supplementary information.<sup>27</sup>

## II. SIMULATION RESULTS

The simulation results are summarized in Figs. 2(a), 2(c), 2(e) and 2(f) for conventional AMOL and in Figs. 2(b), 2(d), 2(g) and 2(h), for reverse-AMOL. As has been described previously, the width of the exposed pattern (and thereby, the lithographic resolution) is inversely proportional to the ratio of the intensities in the two beams,  $I_2/I_1$ . The nature of this inverse relationship is determined primarily by the ratio of the quantum efficiencies of the two photo-reactions occurring inside the AML. As indicated in Fig. 2(a),  $I_2/I_1 > 2000$  is required to achieve a minimum feature size of  $\sim 50$ nm for conventional AMOL. In comparison, a similar minimum feature size can be achieved with  $I_1/I_2 = 2$  in the case of reverse-AMOL as indicated in Fig. 2(b). This is due to the fact that the “confining” reaction in this case is much more efficient than the “exposing” reaction and therefore, requires lower intensity in the “confining” beam. Detailed listing of the parameters of the simulations are included in the supplementary information.<sup>27</sup>

However, it is important to note that the ratio of quantum yields is not the only parameter that affects the minimum feature size. The aperture formation inside the AML is affected by two

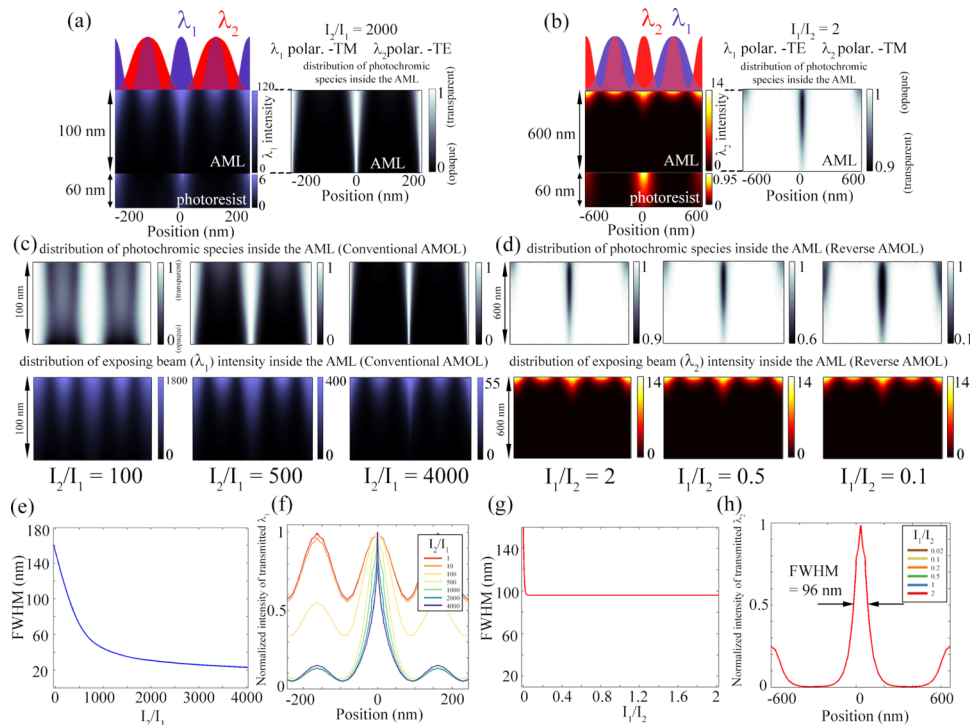


FIG. 2. Simulation results for the (a) conventional AMOL process. Reprinted with permission from AIP Advances 6, 035210 (2016). Copyright 2016 Author(s), licensed under a Creative Commons Attribution 4.0 License. (b) Simulation results for the reverse AMOL process showing the intensity distribution ( $\lambda_2$ ) of the writing beam and the distribution of the photochromic molecules inside the AML. Modulation of the writing beam and the photochromic species distribution inside the AML for different intensity ratios for (c) conventional and (d) reverse AMOL. (e) FWHM (nm) v/s  $I_2/I_1$  for conventional AMOL. Reprinted with permission from AIP Advances 6, 035210 (2016). Copyright 2016 Author(s), licensed under a Creative Commons Attribution 4.0 License. (f) Transmitted exposing beam point spread function (PSF) for conventional AMOL. Reprinted with permission from AIP Advances 6, 035210 (2016). Copyright 2016 Author(s), licensed under a Creative Commons Attribution 4.0 License. (g) FWHM (nm) v/s  $I_2/I_1$  for conventional AMOL. (h) Transmitted exposing beam PSF for reverse AMOL.

phenomena. Firstly, the confinement of the writing beam through the AML is due to the modulation of its absorbance. Hence, the confining beam should be absorbed less compared to the writing beam inside the transparent form in order to maintain the aperture. This means that the ratio of molar absorptivities at the two wavelengths for the “confining” state of the AML,  $\epsilon_{1C}/\epsilon_{2C}$ ,<sup>27</sup> must be greater than or close to 1 for conventional AMOL. For BTE,  $\epsilon_{1C}/\epsilon_{2C} = 0.52$  ( $<1$ , but still not too low). On the other hand, for reverse-AMOL, this ratio is  $\epsilon_{2O}/\epsilon_{1O} = 0.00507$ , which turns out to be too low to create good absorbance contrast and a well-defined aperture in the AML for minimum features below about 96nm.

The second important parameter is the absorbance contrast at the exposing wavelength at the two states of the AML. This parameter is determined by the molar absorptivity ratio at the writing beam, which is  $\epsilon_{1C}/\epsilon_{1O} = 0.33$  for BTE (conventional AMOL)<sup>27</sup> and  $\epsilon_{2O}/\epsilon_{2C} = 0.0078$  for BTE (reverse-AMOL). Due to the lower absorbance contrast for reverse-AMOL, the achievable minimum feature size is limited to about 96nm for the parameters that we used in our experiments. Detailed explanations of the effect of these parameters on the AMOL process were discussed previously.<sup>21</sup> Figs. 2(c)-2(h) shows the combined effect of these parameters on the conventional and reverse-AMOL process. For conventional AMOL, the FWHM is modulated by  $I_2/I_1$  effectively, with decreasing FWHM value for increasing  $I_2/I_1$ . However, this comes at the cost of high intensity ratios. For the reverse-AMOL process, confinement can be achieved down to  $\sim 100$  nm at very low ratios.

Fig. 2(c) and 2(d) present comparisons between the apertures formed inside the AML for the conventional and reverse AMOL cases for different intensity ratios. Lastly, the modulation of the FWHM with intensity ratio is clearly observed in Fig. 2(e) for conventional AMOL, where sub-50 nm confinement can be achieved for  $I_2/I_1 > 2000$ , whereas, for reverse-AMOL in Fig. 2(g),  $\sim 90$  nm FWHM is obtainable even with  $I_1/I_2 < 1$ , but no further modulation is possible. Fig. 2(f) and 2(h) show the actual point spread function (PSF) data corresponding to Fig. 2(e) and 2(g), respectively.

From the numerical analysis, we expect that in conventional AMOL very high intensities may be employed to minimum feature sizes down to  $\sim 30$  nm.<sup>22-24</sup> However, due to the reasons laid out above, this is not strictly true for reverse-AMOL. As a result, the best confinement we can hope to achieve is about 96nm in reverse-AMOL, which corresponds  $\sim \lambda_2/6$ . It is very interesting to note that confinement in reverse-AMOL can be achieved even for  $I_1/I_2 < 1$  (and therefore, very low powers), and this has been experimentally confirmed as described below.

### III. EXPERIMENTAL RESULTS

The samples used in our experiments were prepared in two parts, one consisting of the BTE layer and the other with the photoresist as shown in Fig. 3(a). These two parts were prepared separately and then adhered to each other. Here, a 60 nm thick film of polyvinyl alcohol (PVA) served as the

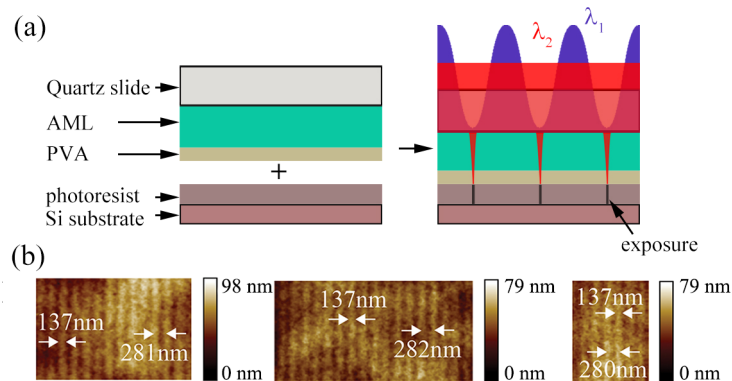


FIG. 3. (a) Schematic of the sample stack. The photoresist is spun onto silicon substrates and the AML is spun on quartz substrates with a thin layer of PVA on top of the AML acting as a barrier layer. The two parts are brought into close contact and then subjected to exposure in the dual wavelength AMOL system. (b) Atomic Force Microscope (AFM) images of the 1D gratings fabricated by reversed AMOL. For all three images,  $\lambda_1$  to  $\lambda_2$  peak intensity ratio  $I_1/I_2$  is 0.139.

barrier layer between the two parts. PVA was chosen as the barrier layer material since it is mostly transparent in the entire wavelength range of interest<sup>28</sup> and can act as an excellent separating layer, while being chemically inert to both the AML and the photoresist. For the first part, a quartz substrate was spin-coated with a monolayer of hexamethyldisilazane (HMDS), 670 nm of AML and 60 nm of PVA acting as barrier layer. The second part of the sample was prepared by spin coating a layer of photoresist (details of the chemical composition of the photoresist have been presented in Ref. 27) on to silicon substrate. The photoresist layer could not be pre-baked, and remained a liquid film. The two parts were then adhered together prior to exposure and then separated after the exposure was concluded. The details of sample preparation and development are described in the supplementary information.<sup>27</sup>

The experiments were performed in a dual-wavelength Lloyd's-mirror interferometer with a standing wave created at  $\lambda_1 = 325\text{nm}$  with a period of  $\sim 280\text{nm}$ , and a uniform illumination at  $\lambda_2 = 647\text{nm}$ .<sup>27</sup> Fig. 3(b) shows atomic-force micrographs of the lines patterned using reverse-AMOL. Three different images were obtained from three different regions of the same sample. The average width of the lines is 137 nm, which is about one fifth of the exposing wavelength (647 nm). The intensity ratio ( $I_1/I_2$ ) used was 0.139. This demonstrates that even with  $I_1/I_2 < 1$ , light confinement could be achieved by reverse-AMOL. Our simulations indicate that with this ratio, the printed feature should be about 100nm. We believe the discrepancy between the experiment and simulation is due to the fact that we do not obtain intimate contact between the AML and the photoresist, which allows the confined beam to diffract slightly before encountering the photoresist. Additionally, we performed simulations to study the effect of line-width broadening for the PSF due to the presence of the PVA barrier layer. This is presented in Fig. S2,<sup>27</sup> which shows considerable spread of the PSF due to increasing barrier layer thickness. When we consider the thickness of the PVA barrier layer (60 nm) and the resulted FWHM broadening, experimental results match pretty well with simulation predications that reversed AMOL can achieve a feature size below 150 nm. Note that the light intensity used here is  $29\text{ W/m}^2$  for  $\lambda_2$  and  $4\text{ W/m}^2$  for  $\lambda_1$ , which is far smaller than that used in a typical AMOL process ( $\sim 1\text{ kW/m}^2$  at  $\lambda_2$ ).

#### IV. CONCLUSION

Due to the limitations of available photochromic molecules, AMOL requires high intensity ratios for sub-diffraction-limited patterning. Here, we demonstrate that this constraint can be overcome by simply reversing the wavelengths of the confining and exposing beams, a technique we refer to as reverse-AMOL. We performed careful simulations to elucidate the key parameters that impact the lithographic resolution of reverse-AMOL and gain the insight that the limiting factor for reverse-AMOL is different than that for conventional AMOL. We further performed experiments by choosing a “red-print” photoresist that exposes in the visible wavelength, but is unaffected by the UV wavelength. Our simulations and experiments suggest that in order to achieve feature sizes below 100nm, further optimization of the absorbance contrast of the photochromic molecule is necessary. Nevertheless, reverse-AMOL is able to achieve feature sizes of about  $\lambda_2/5$  with intensities that are over a magnitude smaller than is required in conventional AMOL.

#### ACKNOWLEDGEMENTS

We would like to thank Chaitanya Ullal for helpful discussions regarding the AML and Brian Baker and Paulo Perez at the University of Utah for assistance with sample imaging. Support from NSF (Grant Number: 1054899) and the Utah Science, Technology and Research (USTAR) initiative are also gratefully acknowledged.

<sup>1</sup> K. Jain, *IEEE Elect. Dev. Meeting* 3(1), 53-55 (1982).

<sup>2</sup> J. G. Maltabes *et al.*, *SPIE Proc.* 1262, 2 (1990).

<sup>3</sup> W. Hinsberg *et al.*, *J. Vac. Sci. Technol. B* 16, 3689 (1998).

<sup>4</sup> H. I. Smith, R. Menon, A. Patel, D. Chao, M. Walsh, and G. Barbastathis, *Microelectron. Eng.* 83, 956-961 (2006).

<sup>5</sup> S. Owa, A. J. Hazelton, and H. H. Magoon, *Microlithogr. World* 16, 4 (2007).

<sup>6</sup> E. Abbé, *Arch. Mikrosk. Anat. Entwicklunsmech* 9(1), 413-418 (1873).

- <sup>7</sup> J. Wu *et al.*, *Langmuir* **31**(17), 5005-5013 (2015).
- <sup>8</sup> S. Natarajan *et al.*, Electron Devices Meeting (IEDM), 2014 IEEE International (2014) pp. 3.7.1-3.7.3.
- <sup>9</sup> B. Haran *et al.*, Electron Devices Meeting (IEDM), 2008 IEEE International (2008) pp. 1-4.
- <sup>10</sup> F. Huo *et al.*, *Nature Nanotech* **5**, 637-640 (2010).
- <sup>11</sup> T. F. Scott *et al.*, *Science* **324**, 913-917 (2009).
- <sup>12</sup> L. Li, R. R. Gattass, E. Gershgoren, H. Hwang, and J. T. Fourkas, *Science* **324**, 910-913 (2009).
- <sup>13</sup> Z. Gan, Y. Cao, R. A. Evans, and Min Gu, *Nature Comm.* **4** **2061**, 1-7 (2013).
- <sup>14</sup> S. W. Hell and J. Wichmann, *Opt. Lett.* **19**(11), 780-782 (1994).
- <sup>15</sup> P. Zimmerman, SPIE Newsroom 1-3 10.1117/2.1200906.1691 (2009).
- <sup>16</sup> X. Luo and T. Ishihara, *Appl. Phys. Lett.* **84**, 4780 (2004).
- <sup>17</sup> X. Fang *et al.*, *Science* **308**, 534-537 (2005).
- <sup>18</sup> P. Gao *et al.*, *Appl. Phys. Lett.* **106**, 093110 (2015).
- <sup>19</sup> R. Menon and H. I. Smith, *J. Opt. Soc. Am. A* **23**(9), 2290-2294 (2006).
- <sup>20</sup> R. Menon, Hsin-Yu Tsai, and S. W. Thomas III, *Phys. Rev. Lett.* **98**(4), 043905-1-4 (2007).
- <sup>21</sup> A. Majumder, P. Helms, and R. Menon, *AIP Advances* **6**, 035210-1-8 (2016).
- <sup>22</sup> T. L. Andrew, H.-Y. Tsai, and R. Menon, *Science* **324**, 917-921 (2009).
- <sup>23</sup> F. Masid, T. L. Andrew, and R. Menon, *Opt. Exp.* **21**(4), 5209-5214 (2013).
- <sup>24</sup> A. Majumder, F. Masid, B. J. Pollock, T. L. Andrew, and R. Menon, *Opt. Exp.* **23**(9), 12244-12250 (2015).
- <sup>25</sup> J. E. Foulkes and R. J. Blaikie, *J. Vac. Sci. Tech. B* **27**, 2941-2946 (2009).
- <sup>26</sup> M. Warner and R. J. Blaikie, *Phys. Rev. A* **80**(3), 03833 (2009).
- <sup>27</sup> See supplementary material at <http://dx.doi.org/10.1063/1.4954178> for details on mathematics related to simulations, sample preparation, optical setup and other details.
- <sup>28</sup> S. D. C. Lowrey and R. J. Blaikie, *J. Micro/Nanolith.* **14**(4), 043510 (2015).